Journal of King Saud University - Science 36 (2024) 103455

HOSTED BY

Contents lists available at ScienceDirect

Journal of King Saud University - Science

journal homepage: www.sciencedirect.com

Full Length Article

Experimental and Statistical approach to understand the adsorption properties of hazardous Cr(VI) on Al_2O_3@$TiFe_2O_4$ nanocomposite: An efficient adsorbent for water treatment

Salman Latif [a], Kaseb D. Alanazi [a], Basmah H. Alshammari [a], Amir Al-Ahmed [b,*], Abdulaziz M. Alanazi [c]

[a] Department of Chemistry, College of Science, University of Ha'il, Ha'il 81451, Saudi Arabia
[b] Interdisciplinary Research Center for Sustainable Energy Systems (IRC-SES), King Fahd University of Petroleum & Minerals (KFUPM), Dhahran 31261, Saudi Arabia
[c] Department of Chemistry, Faculty of Science, Islamic University of Madinah, Madinah 42351, Saudi Arabia

ARTICLE INFO

Keywords:
Metal Oxide Nanoparticle
Adsorption
Langmuir equation
Pseudo-second-order
Statistical physics model

ABSTRACT

Doping of metal oxide with other suitable component can enhance its structural and characteristic properties. At the end it improves its overall application performances. This study introduces the novel synthesis of Al_2O_3@-$TiFe_2O_4$ nanocomposite via co-precipitation for Cr(VI) removal. Unlike previous studies, this unique material exhibits superior adsorption capacity and efficiency. The comparative analysis with existing adsorbents underscores its potential for industrial effluent treatment. The nanocomposite's recyclability and minimal efficiency loss over multiple cycles highlight its sustainability for wastewater treatment. Overall, this research fills existing gaps by presenting an advanced, environmentally friendly adsorbent, significantly enhancing the field of wastewater treatment and environmental remediation. The nanocomposite was characterized and used to study Cr(VI) adsorption characteristics. Amount, contact time, pH, and Cr(VI) concentration were found to influence the adsorption characteristics of the nanomaterial. The operating conditions of an adsorbent Al_2O_3@$TiFe_2O_4$ are optimized utilizing the analysis of the adsorption kinetic data. As shown by the R^2 responses, which were close to unity, the adsorption behaviour of the nanomaterial is in excellent harmony with the linearized Langmuir isotherm with a maximum capacity of 312.52 mg/g. Additionally, Al_2O_3@$TiFe_2O_4$ active sites were more observed to be favorable for Cr(VI) ions at all experimental temperatures range, according to calculations of monolayer adsorption capacities using the Langmuir equation. The value of n was 0.40, 0.42, and 0.43, respectively 25, 35, and 45 °C. The adsorbent shows an adsorption capacity of 93 % with the RSD less than 2 %.

1. Introduction

The Industrial Revolution brought comfort and ease to human life but left a significant environmental consequence: the enormous discharge of polluted wastewater from various industries. This untreated wastewater, often released directly into rivers and other water bodies or on land, severely contaminates groundwater and soil, posing a serious threat to our existence (Ali et al., 2016; Mobarak et al., 2019; Ren et al., 2020). Clean water, essential for human life, irrigation, and many industrial processes, is becoming increasingly scarce (Rathour et al., 2020; Liuyang et al., 2020).

Heavy metals in wastewater are particularly hazardous. When this contaminated water is used for irrigation, heavy metals accumulate in vegetables, grains, and enter the food chain (Jarrah et al., 2020; Islam et al., 2020; Mahmoud et al., 2021; Liu et al., 2023). The rising demand for clean water due to the growing population further exacerbates the problem, and current drinking water resources will soon be insufficient (Loulidi et al., 2023; Essalmi, 2024; Tariq et al., 2022; Mahesh et al., 2023). Additionally, the release of pollutants has disrupted the natural hydrological cycle, and groundwater levels are decreasing alarmingly (Jethave et al., 2022).

Nanotechnology offers a promising solution to water pollution. As an emerging field, nanotechnology has diverse applications, including environmental remediation, energy solutions, and biomedical applications (Jethave and Fegade et al., 2022; Jethave et al., 2019; Jethave et al., 2018). Nanomaterials, with particle sizes less than 100 nm, are

* Corresponding author.
E-mail address: aalahmed@kfupm.edu.sa (A. Al-Ahmed).

https://doi.org/10.1016/j.jksus.2024.103455
Received 7 November 2023; Received in revised form 9 September 2024; Accepted 17 September 2024
Available online 24 September 2024

particularly effective for adsorption-based techniques due to their high surface area, enhancing their physicochemical properties compared to bulk materials (Fegade et al., 2018). Composite nanomaterials, benefiting from synergistic effects, have shown more effectiveness than single nanomaterials for pollutant removal.

Heavy metals, such as arsenic, cadmium, cobalt, and chromium, are highly toxic to living organisms, affecting their internal organs and overall health (Tadjenant et al., 2020; Ren et al., 2020). Chromium (Cr), in particular, is highly toxic and can disrupt the growth of plants and animals, impeding nutrient uptake. Among its various oxidation states, Cr(VI) is the most dangerous, known for its carcinogenic properties (Jethave and Fegade, 2019).

Several studies have explored different materials for Cr(VI) adsorption. Jarrah N. et al. used bentonite-cobalt-layered double hydroxide (Bent-CoAl) to improve Cr(VI) adsorption significantly (Jarrah et al., 2020). Md. Aminul Islam et al. examined various materials like Burneside, pyrolusite, boehmite, and Mn-Al binary oxide under different conditions, finding that surface characteristics, pH, and Cr(VI) concentrations influence adsorption capacity. Ahmed S. Mahmoud et al. synthesized bimetallic Fe/Cu nanoparticles (Fe/Cu NPs), achieving substantial Cr(VI) removal under optimal conditions (Liu et al., 2023). Loulidi et al. used synthetic activated carbon, demonstrating high Cr(VI) adsorption efficiency (Loulidi et al., 2023).

In this study, we synthesized a novel nanocomposite, Al_2O_3@$TiFe_2O_4$, using the co-precipitation method to enhance performance and stability. The synthesized nanocomposite was thoroughly characterized for its structural and morphological properties. We evaluated its Cr(VI) adsorption capacity under varying parameters, finding an impressive adsorption capacity of 312.52 mg/g and excellent reusability. This research addresses the critical need for effective and sustainable solutions for industrial wastewater treatment, highlighting the potential of Al_2O_3@$TiFe_2O_4$ nanocomposite in environmental remediation.

2. Experimental

2.1. Materials and Instrumentation

Analytical reagent-grade chemicals and double distilled water (DDW) were used for this experiment. $AlCl_3{\cdot}6H_2O$ ($\geq$ 99.0 % Pure), $TiCl_4$ (Purity: $\geq$99.9 %) and $FeCl_3$ (Purity: $\geq$98 %) were of Sigma-Aldrich. Potassium dichromate ($K_2Cr_2O_7$), phthalic acid, and 1,5-diphenyl carbohydrazide (DPC) were also obtained from Sigma-Aldrich. DPC reagent was prepared by dissolving phthalic acid (12 g) and 0.75 g of 1,5-diphenyl carbohydrazide (0.75 g) in ethanol (300 mL). The adsorbent was characterized by the Equip-Tronics model EQ 610 Digital pH-meter, the Hitachi SU8010 Field FE-SEM, the Jeol Jem 2100 Plus High-Resolution TEM, EDX performed on the same instrument at 30 kev, the Bruker D8-Advance X-ray diffractometer, Bruker Alpha FTIR, and the Shimadzu UV mini-1240 spectrophotometer.

2.2. Preparation of Al_2O_3@$TiFe_2O_4$ nanocomposite

The synthesis of the Al_2O_3@$TiFe_2O_4$ nanocomposite involved a meticulous procedure to ensure the formation of a high-quality adsorbent material. Firstly, analytical reagent-grade chemicals including $AlCl_3{\cdot}6H_2O$, $TiCl_4$, and $FeCl_3$ were carefully measured in appropriate ratios (4:61:35). These precursor salts were then mixed homogeneously in a 500 mL beaker under constant stirring to achieve a uniform distribution. The temperature of the mixture was gradually raised to 75 °C to facilitate the reaction while maintaining the stability of the solution. Subsequently, a controlled amount of 0.5 M NaOH solution was slowly added to the beaker, resulting in the precipitation of the desired nanocomposite material. The formed precipitate was then subjected to thorough washing to remove any impurities or by-products. After washing, the material was dried to remove excess moisture, followed by calcination at 400 °C for 3 h to stabilize its structure. The resulting nanocomposite material was carefully ground into a fine powder to ensure uniformity and maximize surface area, thus enhancing its adsorption properties.

2.3. Cr(VI) removal study

In a batch adsorption absorption process, Cr(VI) ion removal from aqueous solution were performed. This systematic approach helps to determine the optimal adsorption conditions for maximum efficiency. Initially, varying doses of the nanocomposite material (ranging from 0.20 to 2 g/L) were added to separate batches of chromium-containing solutions with 100 rotations per min for different contact times (ranging from 5 to 90 min). The kinetics of chromium adsorption were monitored closely to understand the rate at which the ions were being captured by the adsorbent material. Effect of solution pH on the adsorption process was also investigated by varying the pH of the solutions from 2.0 to 10 by keeping other parameters (adsorbent dose and time contact) constant. All experiment was repeated 3 times to ensure the reproducibility and reliability of the results. Finally, the Cr(VI) ions adsorption capacity of the nanocomposite was determined under all these variable parameters. These batch adsorption studies provided valuable insights into the adsorption behavior and mechanism of the synthesized nanocomposite material, thereby guiding its potential applications in environmental remediation and wastewater treatment processes.

2.4. Studying isotherm, kinetic and thermodynamic study

Thermodynamic and kinetic isotherm are important tools to understand the mechanism of adsorptions properties of an adsorbent (Dastgerdi et al., 2019; Crini et al., 2008; Jethave et al., 2022, Weber, et al., 1974). Necessary equations used for this study are given in the supplement file.

2.5. Statistical study

Statistical physics-based monolayer to multilayer adsorption models are used to study and determine the adsorption layers of the adsorbent. When it comes to mass transfer, measurement, and the interpretation of experimental data, the application of mathematical modeling and process simulation can be extremely helpful.

$$Q = \frac{nD_m}{1 + \left(\frac{C_{1/2}}{C}\right)^n} \quad \text{(Model 1)}$$

Here, D_m is receptor site's density; n is amount of chromium absorbed by the nanocomposite's active site and adsorbents with concentration $C_{1/2}$ are half-saturated.

$$Q = n.D_m \frac{\left(\frac{C}{C_1}\right)^n + 2\left(\frac{C}{C_2}\right)^{2n}}{1 + \left(\frac{C}{C_1}\right)^n + \left(\frac{C}{C_2}\right)^{2n}} \quad \text{(Model 2)}$$

where concentrations C_1 and C_2 are at the first- and second-layer half-saturation, respectively.

$$Q_a = \frac{\left[n^{*}D_M^{*} \frac{-2\left(\frac{c}{C_1}\right)^{2n}}{\left(1-\left(\frac{c}{C_1}\right)^{n}\right)} + \frac{\left(\frac{c}{C_1}\right)^{n}\left(1-\left(\frac{c}{C_1}\right)^{2n}\right)}{\left(1-\left(\frac{c}{C_1}\right)^{n}\right)^{2}} + 2\frac{\left(\frac{c}{C_1}\right)^{n}\left(\frac{c}{C_2}\right)^{n}\left(1-\left(\frac{c}{C_2}\right)^{nN_2}\right)}{\left(1-\left(\frac{c}{C_2}\right)^{n}\right)} - \frac{\left(\frac{c}{C_1}\right)^{n}\left(\frac{c}{C_2}\right)^{n}\left(\frac{c}{C_2}\right)^{nN_2}N_2\left(1-\left(\frac{c}{C_2}\right)^{n}\right)}{\left(1-\left(\frac{c}{C_2}\right)^{n}\right)} + \frac{\left(\frac{c}{C_1}\right)^{n}\left(\frac{c}{C_2}\right)^{2n}\left(1-\left(\frac{c}{C_2}\right)^{nN_2}\right)}{\left(1-\left(\frac{c}{C_2}\right)^{n}\right)^{2}} \right]}{\frac{\left(1-\left(\frac{c}{C_1}\right)^{2n}\right)}{\left(1-\left(\frac{c}{C_1}\right)^{n}\right)} + \frac{\left(\frac{c}{C_1}\right)^{n}\left(\frac{c}{C_2}\right)^{n}\left(1-\left(\frac{c}{C_2}\right)^{nN_2}\right)}{\left(1-\left(\frac{c}{C_2}\right)^{n}\right)}}$$

(Model 3)

Here, the complete adsorbed layers can be denoted as Nc = 1 + N_2 (Layer).

2.6. Adsorption studies by batch process

The batch adsorption studies were conducted to evaluate the efficacy of the synthesized nanocomposite material in removing Cr(VI) ions from aqueous solutions. A systematic approach was employed to determine the optimal adsorption conditions for maximum efficiency. Initially, varying doses of the nanocomposite material (ranging from 0.20 to 2 g/L) were added to separate batches of chromium-containing solutions. These solutions were then subjected to agitation at 100 rotations per min for different contact times, ranging from 5 to 90 min. The kinetics of chromium adsorption were monitored closely to understand the rate at which the ions were being captured by the adsorbent material. Additionally, the effect of solution pH on the adsorption process was investigated by adjusting the pH of the solutions within a range of 2.0 to 10, while keeping the adsorbent dose and contact time constant. Each experiment was conducted in triplicate to ensure the reproducibility and reliability of the results. The adsorption capacity of the nanocomposite material under various conditions was determined by analyzing the concentration of Cr(VI) ions remaining in the solution after adsorption using suitable analytical techniques. These batch adsorption studies provided valuable insights into the adsorption behavior and mechanism of the synthesized nanocomposite material, thereby guiding its potential applications in environmental remediation and wastewater treatment processes.

3. Results and discussion

3.1. Characterization of Al_2O_3@$TiFe_2O_4$

The average size range of Al_2O_3@$TiFe_2O_4$ nanocomposite is 20.79 nm and a minor aggregation, the nanocomposite is shown to be arranged as circular particles, but the surface is not fully plane, as observed in SEM images (Fig. 1a). However, as seen in Fig. 1a the particle densities are regular. The adsorption process benefits from this uniform crystal structure. The TEM image of the synthesized Al_2O_3@$TiFe_2O_4$ nanocomposite is shown in Fig. 1b to confirm the size of the nanoparticles. In Fig. 1c, before and after adsorption of Cr(VI) the powder X-ray diffraction (XRD) patterns of Al_2O_3@$TiFe_2O_4$ are depicted, revealing characteristic peaks at specific angles. The alignment of XRD peaks for each metal can be accomplished by referencing the Joint Committee on Powder Diffraction Standards (JCPDS) files. This alignment aids in identifying the crystallographic phases present in the material. Before adsorption the observed peaks at angles 5.03° and 2.71° correspond to the characteristic peaks of aluminum oxide (Al_2O_3) according to the JCPDS-ICDD File No 46–1212 (Feret, 2000). These peaks signify the presence of the cubic lattice structure of Al_2O_3. The peaks at angles 24.35°, 27.65°, 36.65°, 48.95°, and 53.15° can be attributed to the titanium ferrite ($TiFe_2O_4$) phase. By referencing the JCPDS file number 04–008-6392 for $TiFe_2O_4$, these peaks align with the hexagonal lattice structure of $TiFe_2O_4$ (Nouh, 2019). Therefore, the XRD analysis confirms that the synthesized Al_2O_3@$TiFe_2O_4$ nanocomposite comprises both phases, as indicated by the alignment of peaks with the respective JCPDS files. After adsorption peak at 24.56° is close to the peak at 24.35° before adsorption, suggesting the retention of a similar phase, possibly indicating minimal structural change at this angle and the peak at 47.12° is not directly matching any of the original peaks but close to 48.95°, suggesting a shift in the peak position due to structural changes or interaction with Cr(VI). The peaks at 24.35° shifted to 24.56°, indicating a slight change in the lattice parameters. This could be due to the incorporation or adsorption of Cr(VI) ions into the lattice structure, causing minor distortions. The original peak at 48.95° shifted to 47.12°, indicating a significant change in the lattice structure, possibly due to Cr (VI) adsorption affecting the crystal lattice or forming a new phase. Peaks at 27.65°, 36.65°, and 53.15° disappeared after adsorption, suggesting possible phase transformations, dissolution of specific crystallographic planes, or masking by the adsorbed Cr(VI) layer. The shifts and disappearance of peaks indicate that the crystalline structure of the AlFeTi oxide nanoparticles is altered upon adsorption of Cr(VI). This can be attributed to the interaction of Cr(VI) with the nanoparticle surface, causing changes in the crystallographic planes. The absence of distinct crystal plane reflections may be due to nanocomposite amorphization, nanostructure effects, and strong interactions at the Al_2O_3/$TiFe_2O_4$ interface, which may obscure traditional crystalline features.

The EDX spectra of the Al_2O_3@$TiFe_2O_4$ in Fig. 1(d) show the sample composition via peaks for Al, Ti, Fe, and O are 0.83, 13.34, 9.10, and 15.19 respectively (Table S1). The results agree with the SAED analyses that were done (Venkatrajan et al., 2018).

Fig. 1e shows the FTIR data.

FTIR Data Before Adsorption

Observed Peaks:

3350 cm^{-1}: Typically associated with O–H stretching vibrations, indicating the presence of hydroxyl groups or adsorbed water.

1628 cm^{-1}: Corresponds to bending vibrations of adsorbed water or N–H bending in amines.

1522 cm^{-1}: Generally associated with C = C stretching in aromatic rings or N-O stretching in nitro compounds.

FTIR Data After Adsorption

Observed Peaks:

3334 cm^{-1}: Slightly shifted from 3350 cm^{-1}, still indicating O–H stretching vibrations, but possibly indicating changes in hydrogen bonding environment or interaction with Cr(VI).

1634 cm^{-1}: Slightly shifted from 1628 cm^{-1}, corresponding to bending vibrations of water or N–H bending, suggesting interaction or coordination with Cr(VI).

Shift from 3350 cm^{-1} to 3334 cm^{-1}: The shift suggests a change in the hydrogen bonding environment, possibly due to the interaction of Cr (VI) with hydroxyl groups on the nanoparticle surface. The presence of

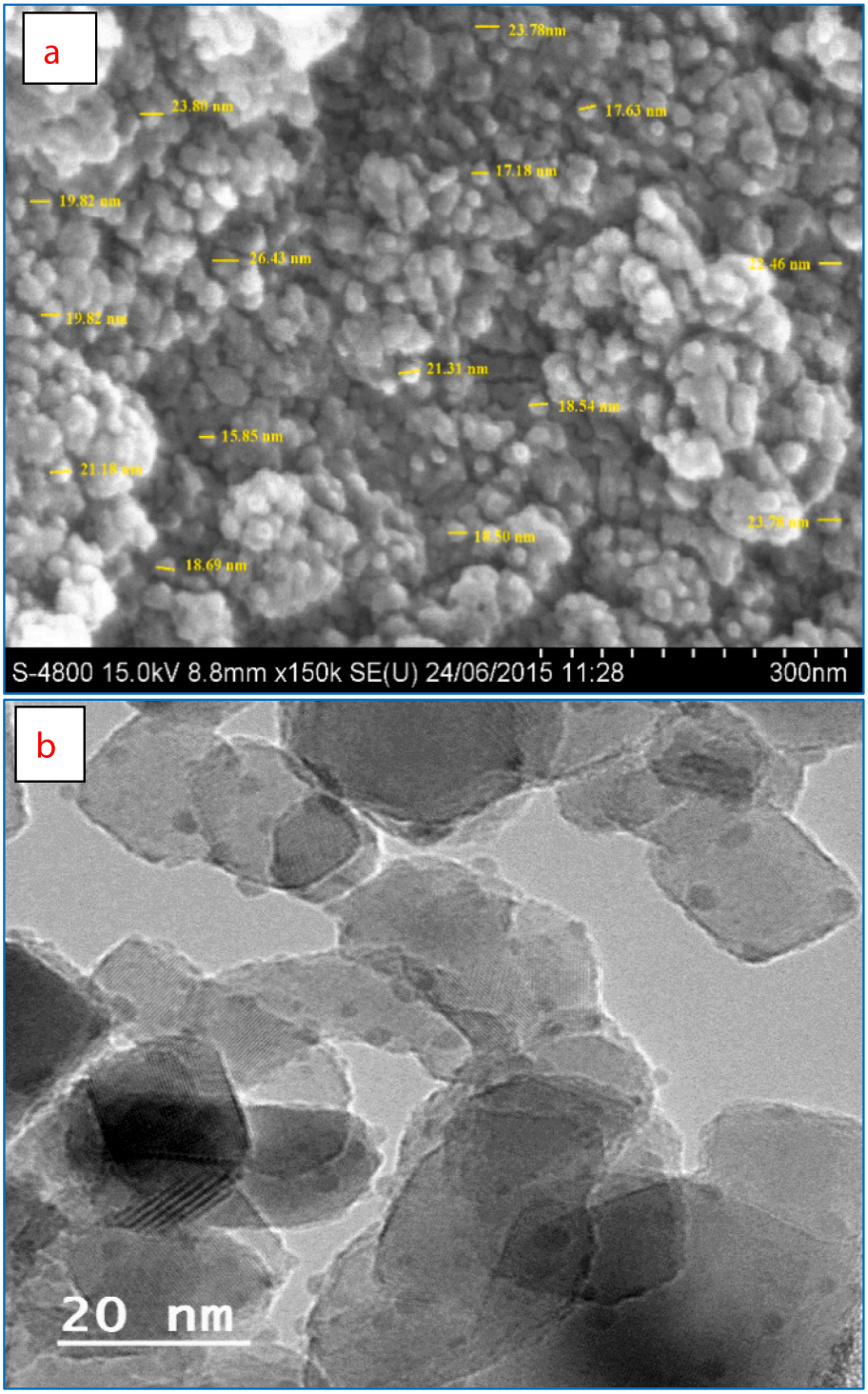

Fig. 1. Morphological characterization results of Al_2O_3@$TiFe_2O_4$ adsorbent, (a) SEM image, (b) TEM images, (c) XRD spectra, (d) EDX spectra, (e) before and after FTIR spectrum.

Cr(VI) could alter the electron density around the O–H groups, leading to a shift in the stretching frequency.

The shift 1628 cm^{-1} to 1634 cm^{-1}: The shift indicates a change in the bending vibrations, likely due to the interaction or complexation of Cr(VI) with functional groups on the nanoparticle surface. This shift could be due to changes in the bonding environment of adsorbed water or amine groups.

The disappearance of this peak 1522 cm^{-1} after adsorption suggests that the functional group responsible for this vibration is either involved in the adsorption process or is altered due to the interaction with Cr(VI). This could indicate that the Cr(VI) ions interact with or disrupt the structure containing aromatic or nitro groups. (Qi et al., 2016).

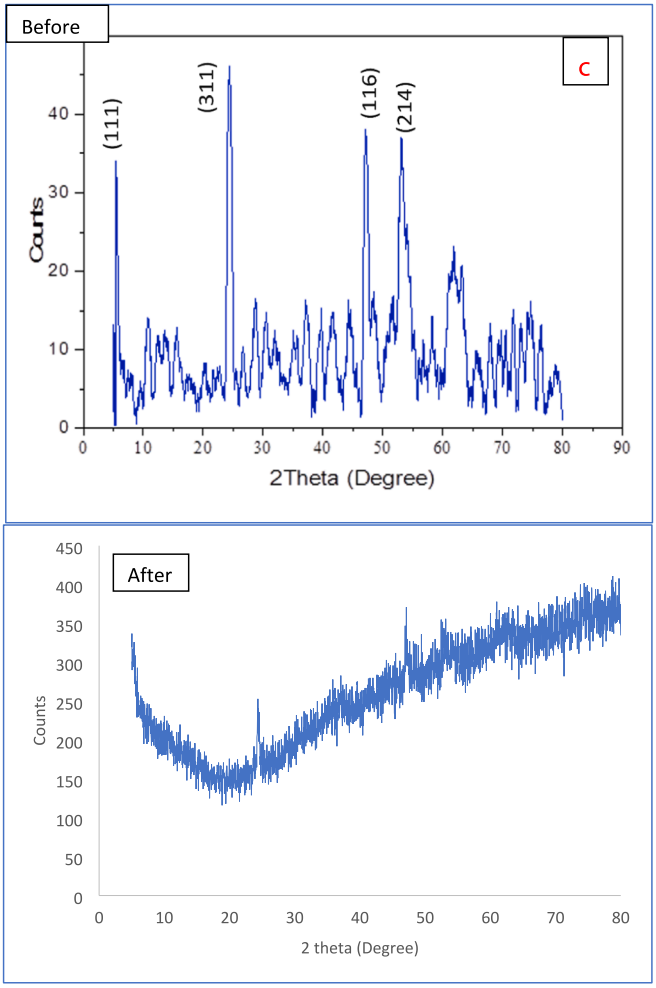

Fig. 1. (*continued*).

3.2. Optimization of Al_2O_3@$TiFe_2O_4$ dose, contact time, pH, Cr(VI) concentration

Different parameters were varied to study adsorption property and to streamline the adsorbent mass. With a fixed Cr(VI) ion concentration of 100 ppm adsorbent property of the of the nanocomposite was investigated with various doses (200–2000 mg) at 25 °C. Fig. 2a shows the effect on the removal efficiency of Cr(VI) with adsorbent *vs.* mass loaded. The optimal productivity of 92.1 % for Cr(VI) evaluation is achieved by using 200 mg of the adsorbent.

Fig. 2b reveals that the nanocomposite is saturated around 60 min and therefore 60 min of contact time is selected as optimum (at 200 ppm and 200 mg). The availability of multiple adsorption sites led to faster adsorption and a Cr(VI) adsorption rate of 84.48 %. The adsorption of Cr (VI) is carried out by pH estimates onto the outer layer of Al_2O_3@$TiFe_2O_4$. Factors, for example, pores, practical hydrogen gatherings, electrostatic attraction, and pH are utilized to oversee the adsorption capability of Cr(VI) particles (Lesaoana, et al., 2019). Fig. 2**c** shows that the ideal pH value obtained for better adsorption is 3.0 and A progressive lowering of the adsorption of Cr(VI) is seen when the pH increases. The presence of hydroxyl groups on the surface of Al_2O_3@$TiFe_2O_4$ in an aqueous solution is responsible for this phenomenon, and the amount of hydroxyl groups changes depending on the pH level. An adsorbent's surface charge reaches neutrality at the point of zero charge (pHpzc). The isoelectric point (pHpzc) of Al_2O_3@$TiFe_2O_4$ is 5 (supplementary figure S1). Anions adhere to the positively charged adsorbent surface when the pH is below the point of zero charge (pHpzc), and the opposite occurs when the pH is above the pHpzc. Raising the pH results in a greater amount of OH^- ions, which then compete with Cr(VI) species (CrO_4^{2-}) for the adsorption sites, leading to a reduction in the adsorption of Cr(VI). When the pH is higher than the point of zero charge (pHpzc), an increase in electrostatic repulsion causes the release of the adsorbed $HCrO_4^-$ and CrO_4^{2-} into the solution (Ko, 2007, Barad, 2022). The chromium ion takes various forms depending on the pH of the solution. Chromate (CrO_4^-) is the most common form of dichromate ($Cr_2O_7^{2-}$) and chromate (CrO_4^-) is the primary type above pH 6.0 at pH 2.0–3.0 of hydrogen chromate ($HCrO_4^-$). In a chromium adsorption component, the numerous chromate particles appear to assume a huge part. Highest adsorption of chromium was achieved at pH 3.0 as displayed in Fig. 2c.

3.3. Kinetics, Isotherm, and Thermodynamic parameters of chromium adsorption

Different active models are utilized to find the adsorption interaction between the adsorbent (Al_2O_3@$TiFe_2O_4$) and the pollutant (Cr(VI)). The adsorption information was assessed on the basis of the pseudo-first, and pseudo-second order models to study the working states the synthesized nanocomposite of an adsorbent. Obtained data confirmed that the adsorption of Cr(VI) suited the pseudo-second-request dynamic model ($R^2 = 0.999$) (Table 1 and Fig. 3**a**). The best fitting in the experimental findings is tracked using the three standard isothermal models Langmuir, Freundlich, and Temkin. While monolayer adsorption occurs on a heterogeneous surface with varying strengths in Freundlich, it does so on a uniform surface with the same attraction and energy in Langmuir

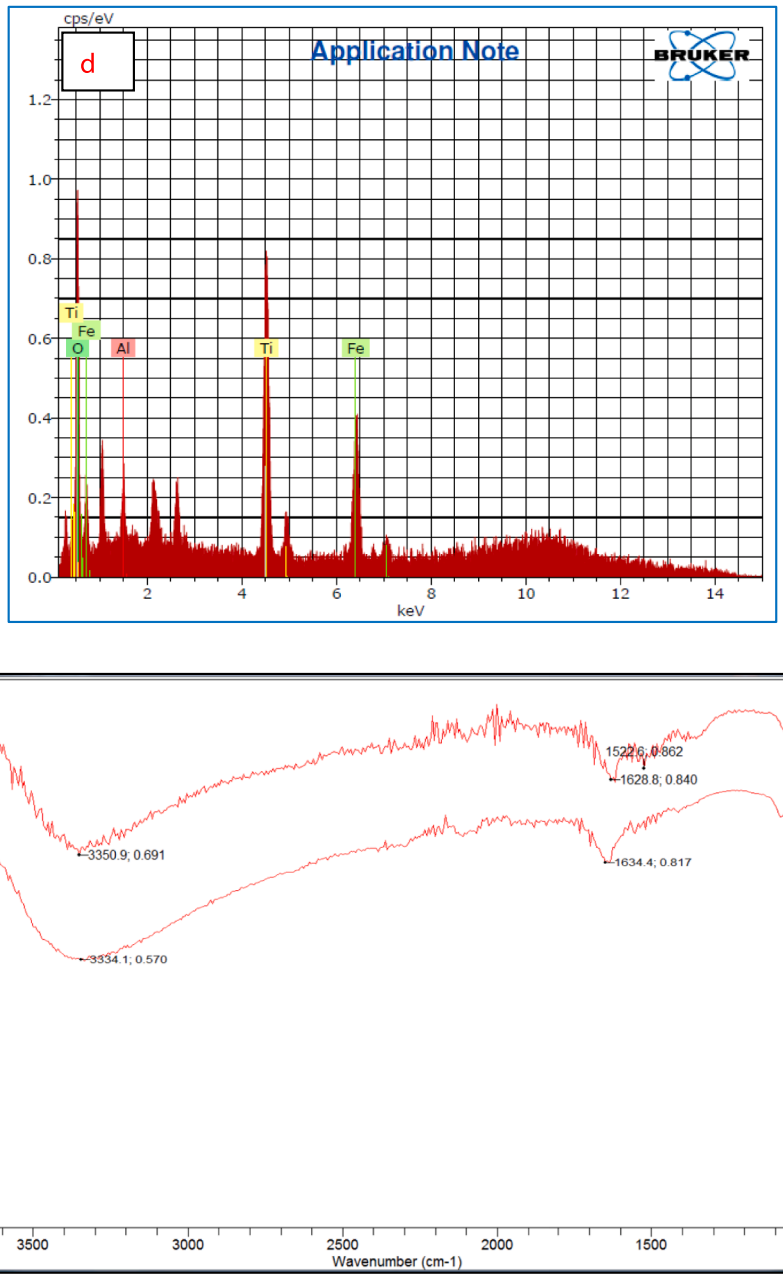

Fig. 1. (*continued*).

(Langmuir, 1918). The linearized isotherm and separation factor models for Cr(VI) adsorption onto Al_2O_3@$TiFe_2O_4$ are displayed in Fig. 3**b-3e**. Table 1 also provides a summary of the calculated isotherm parameters for Cr(VI) adsorption onto Al_2O_3@$TiFe_2O_4$ derived from linearized isotherm models. The adsorption behavior of the Al_2O_3@$TiFe_2O_4$ determined by Freundlich and Temkin are in concurrence with their linearized Langmuir isotherm model, as the R^2 values are approaching solidarity (Freundlich and Heller, 1939). For the Langmuir, Temkin and Freundlich isotherm models, the R^2 values are approximately 0.996, 0.9888, and 0.9674, respectively. Results propose that Cr(VI) is consistently circulated on the outer layer of Al_2O_3@$TiFe_2O_4$ during compound harmony. With the Langmuir isotherm model, all adsorption locales on the outer layer of the adsorbent are indistinguishable and just a single kind of communication happens between the Al_2O_3@$TiFe_2O_4$ and every adsorbate. The calculated maximum adsorption capacity of Al_2O_3@$TiFe_2O_4$ for Cr(VI) is about 312.52 mg/g.

Between 25 and 45 °C, researchers studied how temperature affected Cr(VI) adsorption onto Al_2O_3@$TiFe_2O_4$. Cr(VI)'s thermodynamic parameters are calculated (Pierott et al., 1974; Lei et al., 2020; Lotfi et al., 2019). At three different temperatures of 25, 35, and 45 °C, the Cr(VI) adsorption onto the surface of Al_2O_3@$TiFe_2O_4$ is examined under advanced conditions. The unrestricted course of Cr(VI) adsorption is advised by the negative value of ΔG°. The negative value of ΔH°, it can be inferred from Table 1 that the adsorption process is exothermic. Additionally, the observed positive value of ΔS° indicates an increase in entropy after the removal of Cr(VI) at the solid/solution interface.

3.4. Statistical analysis

Fig. 4. presents the application of physics models towards the adsorption isotherms of Cr(VI) on the nanocomposite in different temperature. The experimental data are also found to be well-fitted in this

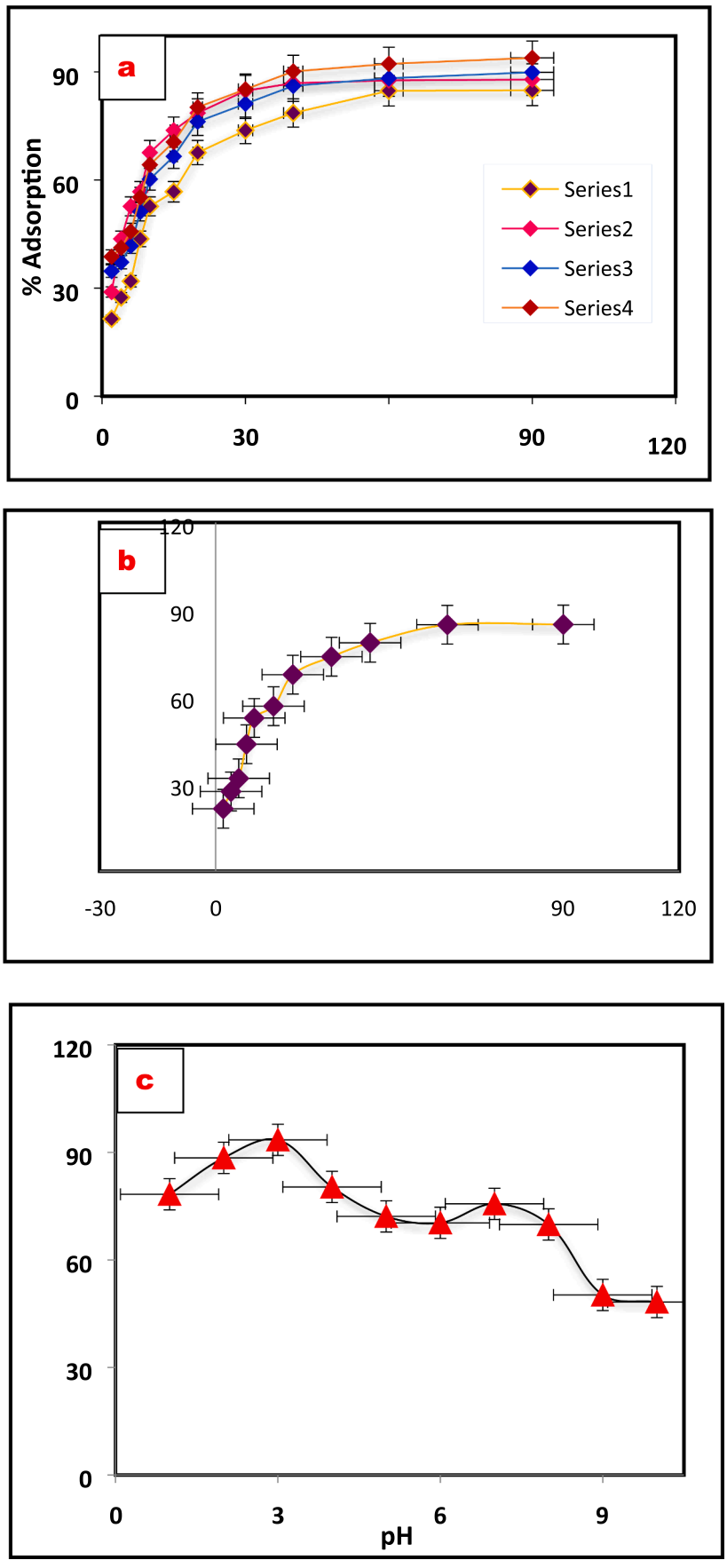

Fig. 2. Adsorption properties of the Al_2O_3@$TiFe_2O_4$. adsorbent, (a) Cr(VI) dose, (b) contact time and (c) solution pH optimization.

Table 1
The parameters showing pseudo-second-order kinetics, Isotherm, Gibbs and Enthalpy of formation studies of Cr(VI) adsorption by Al_2O_3@$TiFe_2O_4$ nanocomposite.

Pseudo-second order kinetic Model								
Concentration (ppm)			50			100	150	200
K			0.106			0.108	0.104	0.104
Qe			1.061			1.613	2.315	9.259
R^2			0.997			0.999	0.998	1.000
Langmuir			**Freundlich**			**Temkin**		
qmax (mg/g)	**R_L**	**R^2**	**K_f (mg/g)**	**1/n**	**R^2**	**B (KJ mol^{-1})**	**K_T (L/mg)**	**R^2**
312.5	0.016	0.9961	11.11	0.577	0.9674	1.7848	1.008	0.9888
Thermodynamic parameter								
Temperature (K)		**298**			**308**		**318**	
ΔG° (KJ/mol)		−4.128			−4.770		−5.428	
ΔH° (KJ/mol)					**ΔS° (J/mol K)**			
−0.008314					−0.03326			

instance. Here the results of the Al_2O_3@$TiFe_2O_4$ nanocomposite (Model 2) to fit the Cr(VI) adsorption isotherms to the best possible fitting models. Table 2 demonstrates that the double layer model (Models 2) uses parameters such as n, NM, Q_{sat}, ε_1, ε_2 for Cr(VI) adsorption on Al_2O_3@$TiFe_2O_4$.

The mathematical orientation of the captured Cr(VI) particles on the Al_2O_3@$TiFe_2O_4$ composite surface (horizontal or vertical) and the system (multi-docking and multi-ionic) are not fixed it is depending the value of n. The horizontal orientation and multi-docking mechanism are associated with $n = 1$, while the vertical orientation and multi-molecular behavior are associated with $n = 2$. The n values 0.40, 0.42, and 0.43 were calculated at 25, 35, and 45 °C, respectively shown the horizontal orientation and multi-docking mechanism. When $n < 1$, a multimolecular bond may be explained by several active sites adsorbing a single molecule or ion, however when $n > 1$, a multimolecular bond can be explained by a single active site adsorbing many molecules or ions. Fig. 5**a** shows how the value of n changed with temperature, and Table 2 lists the results of mathematical comparisons (Lotfi and Franco et al., 2019, Jethave et al 2017).

Cr(VI) adsorption follow horizontal orientation on the surface of nanoparticle. For Cr(VI)-Al_2O_3@$TiFe_2O_4$ adsorption, parameter n is determined and recorded as a temperature-dependent on thermal movement in a decrement order (0.364 to 0.358). It should be mentioned that the Cr(VI)-Al_2O_3@$TiFe_2O_4$ aggregates in the solution lose their bond around 318 K, which reduces the development of layers on the adsorbent's surface.

The effect of temperature on the density of receptor sites (Nm) is shown in Fig. 6b. This boundary uncovered the contrary example of the boundary n. Fundamentally, the accessible region on the Al_2O_3@$TiFe_2O_4$ surface might be expanded, and subsequently the quantities of fortified Cr(VI) particles on the dynamic locales are decreased because of the accessibility of extra dynamic destinations.

Fig. 5**b** shows the barrier affects arrangement temperature in single-compound and double frameworks. Temperature increased Cr(VI) and Al_2O_3@$TiFe_2O_4$ adsorption receptor site density (N_M) in the two systems under study. N_M increased due to a temperature-dependent expansion effect in the Al_2O_3@$TiFe_2O_4$ structure that created new active sites (Elhadj et al. 2020, Jethave et al., 2022). The exothermic effect that was discovered through the analysis of the experimental data is in line with this outcome. As depicted in Fig. 5**b**, an increase in the adsorbed quantity was accompanied by an increase in the N_M value, mirroring the control of the new vacant Al_2O_3@$TiFe_2O_4$ dynamic destinations by the adsorbed particles. This confirmed that Cr(VI) adsorption is more specific to Al_2O_3@$TiFe_2O_4$ dynamic destinations.

The Langmuir model is used to study Cr(VI) adsorption from aqueous solutions onto Al_2O_3@$TiFe_2O_4$. No matter the adsorbent, this conventional model holds that the only way Cr(VI) can be adsorbed is through the formation of an adsorbed sheet. At long last, the last fascinating physicochemical boundary is the absolute number of soaked Al_2O_3@$TiFe_2O_4$ particles. Q_{sat} (for instance, Q_{esat} = N*Nm and the model with two-fold layer Q_{sat} = 2 N*Nm) observed to decrease as the experimental temperature increases (Fig. 5**c**), which is now confirmed in the explanation of trial data. Calculating the adsorption energy of two practical groupings helps explain the Cr(VI) expulsion procedure. The following formulas quantify half-saturation concentration adsorption energies at 298–328 K, where the energy of adsorption is determined by the following equations.

$$\hat{I}\mu_1 = \mathrm{RT}\ln\left(\frac{C_S}{C_1}\right) \quad (1)$$

$$\hat{I}\mu_2 = \mathrm{RT}\ln\left(\frac{C_S}{C_2}\right) \quad (2)$$

Here, Cs is the solubility of Cr(VI), T is the temperature, and R is the ideal gas constant. These energies in both functional classes when El > E2 represent an exothermic chemisorption.

Adsorption energies (E) values are shown in Fig. 5**d** for all solution temperatures (25, 35, and 45 °C). At 25, 35, and 45 °C, the El displayed values of 20.05, 22.76, and 23.91 $kJmol^{-1}$. The values of the E2 at the same succession of solution temperatures were 10.91, 3.58, and 10.15 (Table 2**)**. As a result, the Al_2O_3@$TiFe_2O_4$ adsorbent's active sites were better able to absorb hexavalent Cr ions due to the adsorption energy (i.e., the Qsat and had the same trend with temperature) (Ibrahim et al. 2019). Additionally, the Cr(VI) ion adsorption onto Al_2O_3@$TiFe_2O_4$ was related to uptake energies that were all 40 $kJmol^{-1}$, indicating a physical component to the adsorption phenomenon. It was evident that a larger adsorption energy indicates the second functional group's binding contact, proving their significant role in the elimination of Cr(VI) ions. The Al_2O_3@$TiFe_2O_4$ and Cr(VI) adsorbents previously described in the literature are compared in Table 2.

3.5. Mechanism

To provide a comprehensive understanding of the adsorption mechanism considering pH and other results, we need to consider various factors such as the surface chemistry of the adsorbent, the chemical properties of the adsorbate, and the influence of pH on the adsorption process. The Al_2O_3@$TiFe_2O_4$ nanocomposite possesses active surface sites due to its composition of aluminum oxide (Al_2O_3) and titanium ferrite ($TiFe_2O_4$). These surface sites play a crucial role in adsorbing chromium ions (Cr(VI)) from the solution. pH significantly

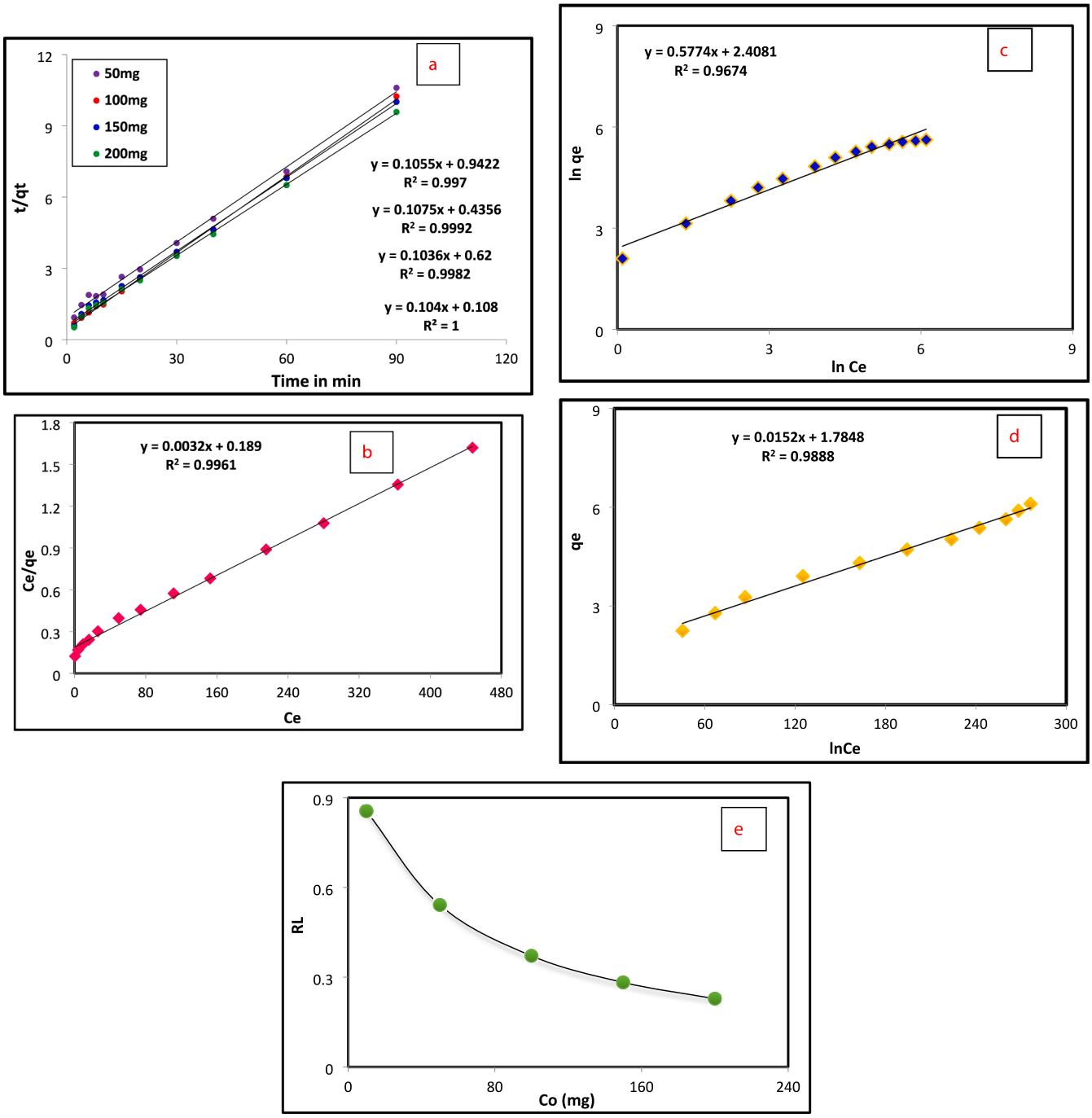

Fig. 3. A) pseudo second order kinetic (b) langmuir (c) freundlich (d) temkin isotherm, (e) separation factor of cr(vi) adsorption by al_2O_3@$TiFe_2O_4$ nanocomposite.

affects the surface charge of both the adsorbent and the adsorbate species. At lower pH values, the surface of the Al_2O_3@$TiFe_2O_4$ nanocomposite is positively charged due to protonation of surface hydroxyl groups, while Cr(VI) ions are predominantly present as chromate ions (CrO_4^{2-}) and dichromate ions ($Cr_2O_7^{2-}$) depending on the pH. The positively charged surface of the adsorbent facilitates electrostatic attraction with the negatively charged Cr(VI) species, enhancing adsorption. Under acidic conditions (pH $<$ 7), the predominant Cr(VI) species are dichromate ions ($Cr_2O_7^{2-}$) and chromate ions (CrO_4^{2-}). The positively charged surface of the Al_2O_3@$TiFe_2O_4$ nanocomposite interacts with the negatively charged Cr(VI) species via electrostatic attraction. Additionally, surface complexation reactions may occur between Cr(VI) ions and functional groups present on the adsorbent surface, such as hydroxyl groups and surface oxide species. The adsorption capacity of the nanocomposite for Cr(VI) ions is influenced by factors such as, contact time, adsorbent dosage, and temperature, as determined from batch adsorption studies.

The low ΔH° value indicates that the dominant mechanism is likely electrostatic attraction between the positively charged surface of the Al_2O_3@$TiFe_2O_4$ nanocomposite and the negatively charged Cr(VI) species (e.g., chromate and dichromate ions).

The small negative ΔH° also implies that the process is exothermic but not highly energy-intensive, characteristic of weak interactions typical in physical adsorption.

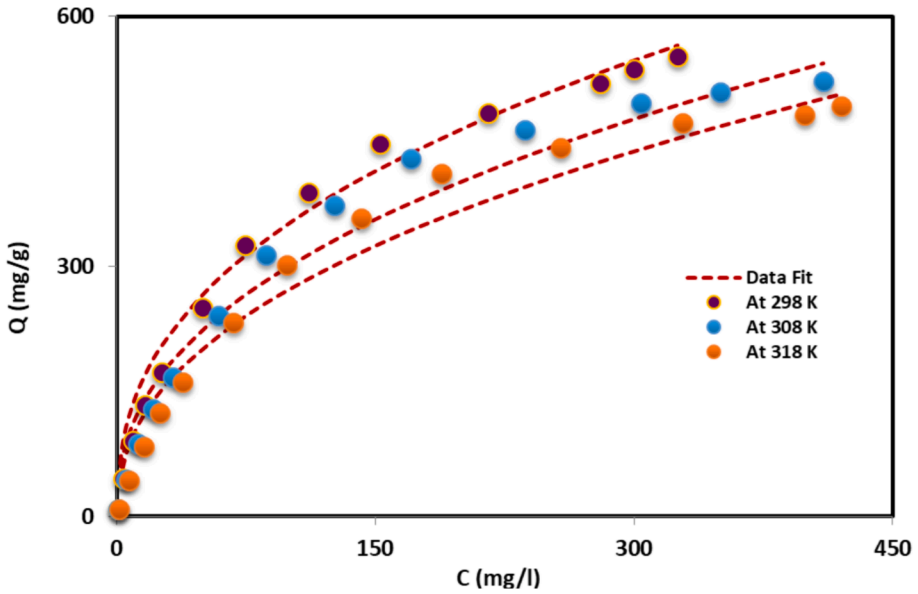

Fig. 4. Fitting of double layer model at different temperatures.

Table 2
Valued obtained by fitting the Model 2.

Temperature (K)	n	N_M (mg/g)	Qsat (mg/g)	C_1	C_2	ε_1 (KJ/mol)	ε_2 (KJ/mol)
298	0.40	410.00	328.00	15.00	600.00	20.05	10.91
308	0.42	227.92	191.69	6.75	12087.75	22.76	3.58
318	0.43	183.34	158.03	5.78	1055.35	23.91	10.15

3.6. Regeneration and application to industrial wastewater

Reusability is one of the significant properties of a good absorbent. The initial objective of this study is to choose cost-effective adsorbents after disposal and to minimize the potential environmental impacts regarding sustainable solid waste management. The reusability studies are performed using the optimized experimental conditions for the adsorption of Cr(VI) on the surface of Al_2O_3@$TiFe_2O_4$. The used adsorbent is successfully gathered using a centrifuge machine and cleaned with HCl (0.1 M) after each adsorption process followed by neutralization with NaOH (0.1 M). A similar process is used after every adsorption cycle. The adsorbent is used for up to five cycles and it is observed that the adsorption efficiency decreases by less than 2 % (Fig. 7 **and** Table 3). The regeneration performance of the adsorbent is almost constant for up to five cycles. This confirms a substantial balance between its ecological effect and its affordability. The % regeneration efficiency is calculated at the end of each cycle, using the following Eq. (3):

$$\text{Regeneration efficiency}\,(\%) = (\text{Amount of desorbed}/\text{Amount of adsorbed}) \times 100 \quad (3)$$

The synthesized Al_2O_3@$TiFe_2O_4$ is successfully adopted for the treatment of chemical, metal and textile industrial effluents containing Cr(VI) to achieve a clean environment and save water by recycling it. The % adsorption for Cr(VI) at 93 % with the RSD less than 2 %. Furthermore, experimental data from this study demonstrated the ability and efficiency of the Al_2O_3@$TiFe_2O_4$ and therefore, it has become an efficient candidate for the treatment of industrial effluents. And superior adsorption capacity as compared to previously reported various adsorbent (Table 4).

The novelty of this work lies in several key aspects that distinguish it from previous studies in the literature, highlighting the significance and necessity of this research:

This study presents the synthesis of a novel nanocomposite material, Al_2O_3@$TiFe_2O_4$, using the co-precipitation method. While previous studies have investigated various adsorbents for Cr(VI) removal, the synthesis of this specific nanocomposite material is novel and offers unique properties for efficient adsorption. Through a comparison with existing adsorbents reported in the literature, this study highlights the superior adsorption capacity and efficiency of the Al_2O_3@$TiFe_2O_4$nanocomposite for Cr(VI) removal. This comparative analysis underscores the significance of the synthesized nanocomposite as a promising candidate for industrial effluent treatment. The investigation of the nanocomposite's recyclability, with minimal decrease in adsorption efficiency over multiple cycles, underscores its potential for sustainable use in wastewater treatment applications. This aspect of the study addresses the need for environmentally friendly and cost-effective adsorbents. Overall, this study addresses the gaps in the existing literature by introducing a novel adsorbent material, elucidating its adsorption mechanism, and demonstrating its superior performance for Cr(VI) removal. By highlighting these aspects, the study underscores the importance and relevance of its findings in advancing the field of wastewater treatment and environmental remediation.

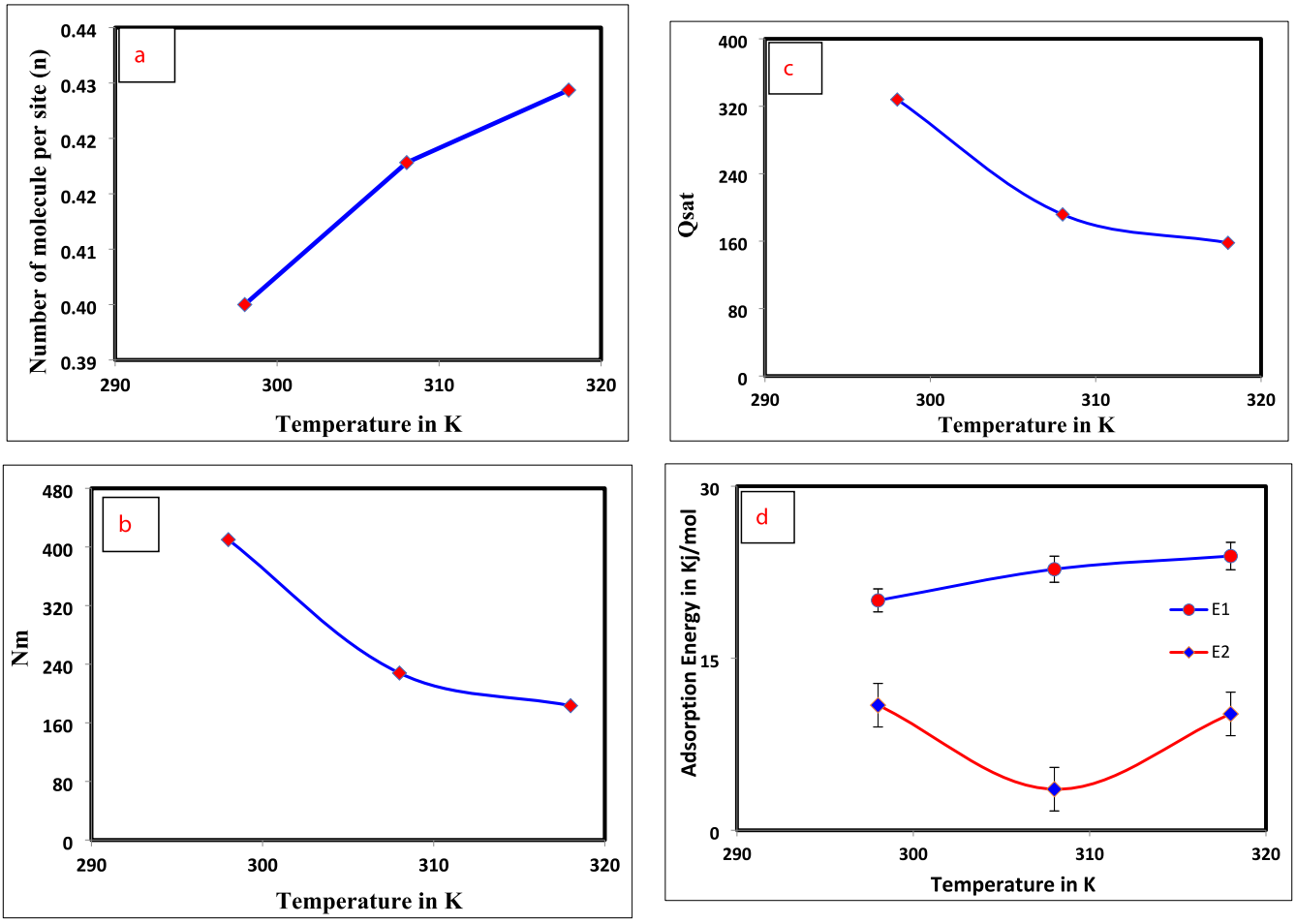

Fig. 5. Temperature dependence parameters are plotted as, (a) n, (b) Nm, (c) $Q_{esat,}$ and (d) Energy of adsorption Vs T (K).

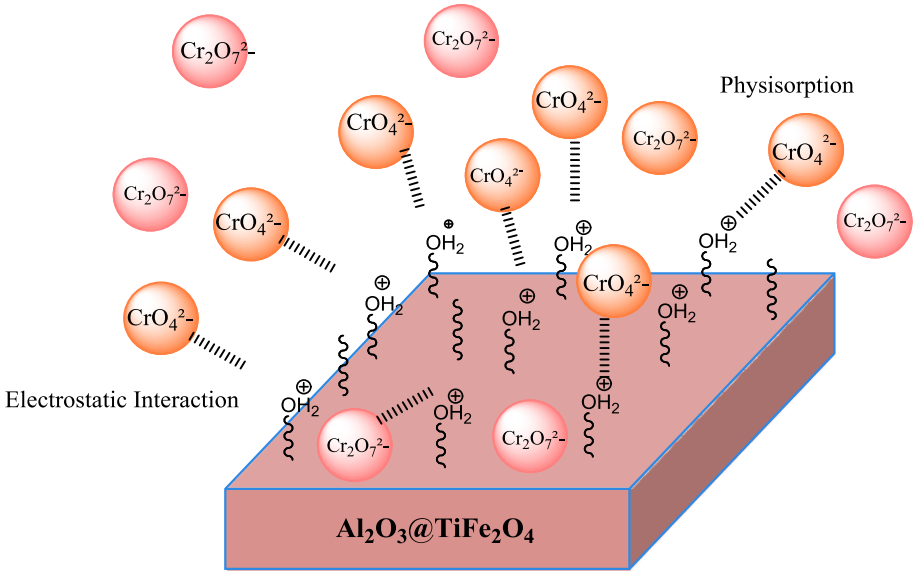

Fig. 6. Schematic Representation of adsorption mechanism.

4. Conclusion

In this study, a novel adsorbent Al_2O_3@$TiFe_2O_4$ was successfully synthesized using co-precipitation method and evaluated for the mono-component adsorption of Cr(VI) under various conditions. The findings shed light on the efficacy of this adsorbent for the removal of Cr(VI) from aqueous solutions. Adsorption capacity of Cr(VI) reached its maximum at pH 3, indicating the significant influence of ion exchange interactions

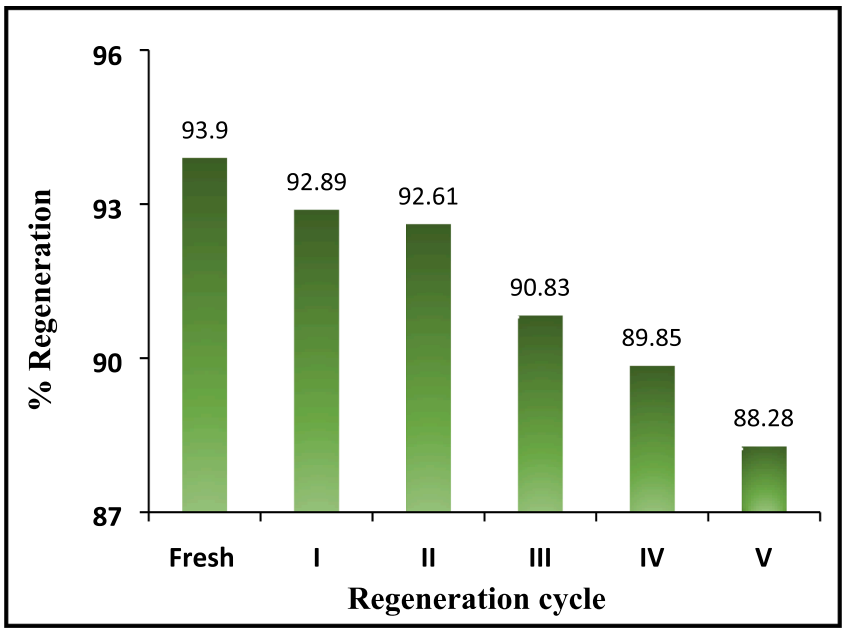

Fig. 7. Regeneration study (for 100 mg/L concentration of Cr(VI)).

Table 3
Practical applicability of the Al_2O_3@$TiFe_2O_4$ for the removal of 50 and 100 mg/l industrial effluent Cr(VI).

Cr(VI) (mg/L)	% Adsorbed	Remain unadsorbed %	Cr(VI) remains	Average	SD	RSD
50	93.9	6.1	3.05	93.54	0.36	0.384
50	93.54	6.46	3.23			
50	93.18	6.82	3.41			
100	93.37	6.63	6.63	93.53	0.219	0.234
100	93.78	6.22	6.22			
100	93.44	6.56	6.56			

Table 4
Comparative table of Various adsorbent used for the adsorption of Cr(VI) in recently published literature.

Adsorbent	Maximum Adsorption Capacity (mg/g)	References
Al_2O_3@$TiFe_2O_4$	312.52	This study
Carbon Nanotubes (CNT)	168.54	[Jia, D., 2022]
Activated Carbon (AC)	154.56	[Wang, H., 2023]
Metal-Organic Frameworks (MOFs)	78.12	[Babapour, M., 2022]
Graphene Oxide (GO)	19.49	[Naseem, 2022]
rGO-ZnO nanocomposite	25.45	[Naseem, 2022]
eggshell-based cobalt oxide- zinc oxide nanocomposite	38.32	[Seid, 2022]

in facilitating adsorption onto the Al_2O_3@$TiFe_2O_4$ surface. To optimize the operating parameters of the adsorbent, PFO and PSO models were utilized to analyze the adsorption kinetic data, yielding satisfactory fits with R^2 values close to unity. Further analysis using Langmuir, Freundlich, and Temkin isotherm models revealed excellent agreement between experimental data and model predictions, with R^2 values of approximately 0.998, 0.967, and 0.989, respectively. The calculated maximum adsorption capacity of Al_2O_3@$TiFe_2O_4$ for Cr(VI) was determined to be 312.52 mg/g, indicating its high efficiency in removing Cr (VI) ions from aqueous solutions. Moreover, the adsorption behavior of Cr(VI) onto Al_2O_3@$TiFe_2O_4$ was found to be favorable, with the active sites exhibiting a preference for Cr(VI) ions at all temperatures. The multi-docking mechanism of Cr(VI) interaction with Al_2O_3@$TiFe_2O_4$ was elucidated, indicating the horizontal location of n1 at 25 and 35 °C. Additionally, the adsorbent demonstrated good recyclability, with only a minor decrease in adsorption efficiency observed over five cycles, highlighting its potential for repeated use in industrial effluent treatment processes. The application of synthesized Al_2O_3@$TiFe_2O_4$ holds promise for achieving efficient Cr(VI) removal, contributing to environmental sustainability and water conservation efforts. Overall, the study achieved a remarkable Cr(VI) adsorption efficiency of 93 %, with a relative standard deviation (RSD) of less than 2 %, underscoring the effectiveness and reliability of Al_2O_3@$TiFe_2O_4$ as a viable solution for Cr(VI) removal from contaminated water sources.

Availability of data and materials

Not Applicable.

CRediT authorship contribution statement

Salman Latif: Writing – review & editing, Investigation, Funding acquisition, Conceptualization. **Kaseb D. Alanazi:** Writing – original draft, Supervision, Resources, Formal analysis, Data curation. **Basmah H. Alshammari:** Writing – original draft, Software, Resources, Investigation, Data curation, Conceptualization. **Amir Al-Ahmed:** Visualization, Supervision, Project administration, Funding acquisition, Conceptualization. **Abdulaziz M. Alanazi:** Writing – review & editing,

Writing – original draft, Software, Methodology, Investigation, Conceptualization.

Declaration of Competing Interest

The authors declare that they have no known competing financial interests or personal relationships that could have appeared to influence the work reported in this paper.

Acknowledgment

This research has been funded by Scientific Research Deanship at University of Ha'il-Saudi Arabia through project number RG-23 050.

Appendix A. Supplementary material

Supplementary data to this article can be found online at https://doi.org/10.1016/j.jksus.2024.103455.

References

Barad, J.M., Kohli, H.P., Chakraborty, M., 2022. Adsorption of hexavalent chromium from aqueous stream by maghemite nanoparticles synthesized by the microemulsion method. Energy Nexus 5, 100035.
Crini, G., 2008. Kinetic and equilibrium studies on the removal of cationic dyes from aqueous solution by adsorption onto a cyclodextrin polymer. Dyes Pigm. 77 (2), 415–426.
Dastgerdi, Z.H., Meshkat, S.S., Esrafili, M.D., 2019. Enhanced adsorptive removal of Indigo carmine dye performance by functionalized carbon nanotubes based adsorbents from aqueous solution: equilibrium, kinetic, and DFT study. J. Nanostruct. Chem. 9 (4), 323–334.
Elhadj, M., Samira, A., Mohamed, T., Djawad, F., Asma, A., Djamel, N., 2020. Removal of Basic Red 46 dye from aqueous solution by adsorption and photocatalysis: equilibrium, isotherms, kinetics, and thermodynamic studies. Sep. Sci. Technol. 55 (5), 867–885.
Essalmi, S., Lotfi, S., BaQais, A., Saadi, M., Arab, M., Ahsaine, H.A., 2024. Design and application of metal organic frameworks for heavy metals adsorption in water: a review. RSC Adv. 14 (13), 9365–9390.
Fegade, U., Jethave, G., Su, K.Y., Huang, W.R., Wu, R.J., 2018. An multifunction $Zn_{0.3}Mn_{0.4}O_4$ nanospheres for carbon dioxide reduction to methane via photocatalysis and reused after five cycles for phosphate adsorption. Journal of Environmental. Chem. Eng. 6 (2), 1918–1925.
Feret, F.R., Roy, D., Boulanger, C., 2000. Determination of alpha and beta alumina in ceramic alumina by X-ray diffraction. Spectrochim. Acta B At. Spectrosc. 55 (7), 1051–1061.
Franco, D.S., Duarte, F.A., Salau, N.P.G., Dotto, G.L., 2019. Adaptive neuro-fuzzy inference system (ANIFS) and artificial neural network (ANN) applied for indium (III) adsorption on carbonaceous materials. Chem. Eng. Commun. 206 (11), 1452–1462.
Freundlich, H., Heller, W., 1939. The adsorption of cis-and trans-azobenzene. J. Am. Chem. Soc. 61 (8), 2228–2230.
Ibrahim, M.M., 2019. Cr2O3/Al2O3 as adsorbent: physicochemical properties and adsorption behaviors towards removal of Congo red dye from water. J. Environ. Chem. Eng. 7 (1), 102848.
Islam, M.A., Angove, M.J., Morton, D.W., Pramanik, B.K., Awual, M.R., 2020. A mechanistic approach of chromium (VI) adsorption onto manganese oxides and boehmite. J. Environ. Chem. Eng. 8 (2), 103515.
Jarrah, N., Mu'azu, N.D., Zubair, M., Al-Harthi, M., 2020. Enhanced adsorptive performance of Cr(VI) onto layered double hydroxide-bentonite composite: Isotherm, kinetic and thermodynamic studies. Sep. Sci. Technol. 55 (11), 1897–1909.
Jethave, G., Fegade, U., Attarde, S., Ingle, S., 2017. Facile synthesis of Lead Doped Zinc-Aluminum Oxide Nanoparticles (LD-ZAO-NPs) for efficient adsorption of anionic dye: kinetic, isotherm and thermodynamic behaviors. J. Ind. Eng. Chem. 53, 294–306.
Jia, D., Jing, Z., Duan, Y., Li, J., 2022. Ultrafast removal of Cr(VI) ions using polyamine modified carbon nanotubes. J. Taiwan Inst. Chem. Eng. 133, 104265.
Ko, I., Davis, A.P., Kim, J.Y., Kim, K.W., 2007. Effect of contact order on the adsorption of inorganic arsenic species onto hematite in the presence of humic acid. J. Hazard. Mater. 141 (1), 53–60.
Langmuir, I., 1918. The adsorption of gases on plane surfaces of glass, mica and platinum. J. Am. Chem. Soc. 40 (9), 1361–1403.
Lei, C., Wang, C., Chen, W., He, M., Huang, B., 2020. Polyaniline@ magnetic chitosan nanomaterials for highly efficient simultaneous adsorption and in-situ chemical reduction of hexavalent chromium: removal efficacy and mechanisms. Sci. Total Environ. 733, 139316.
Lesaoana, M., Mlaba, R.P.V., Mtunzi, F.M., Klink, M.J., Ejidike, P., Pakade, V.E., 2019. Influence of inorganic acid modification on Cr (VI) adsorption performance and the physicochemical properties of activated carbon. S. Afr. J. Chem. Eng. 28, 8–18.
Liu, J., Sun, S., Zhang, H., Kong, Q., Li, Q., Yao, X., 2023. Remediation materials for the immobilization of hexavalent chromium in contaminated soil: preparation, applications, and mechanisms. Environ. Res. 116918.
Liuyang, X., Yang, H., Huang, S., Zhang, Y., Xia, S., 2020. Resource utilization of secondary pyrolysis oil-based drilling cuttings ash for removing Cr(VI) contaminants: adsorption properties, kinetics and mechanism. J. Environ. Chem. Eng. 8 (6), 104474.
Lotfi, R., Hayati, B., Rahimi, S., Shekarchi, A.A., Mahmoodi, N.M., Bagheri, A., 2019. Synthesis and characterization of PAMAM/SiO_2 nanohybrid as a new promising adsorbent for pharmaceuticals. Microchem. J. 146, 1150–1159.
Loulidi, I., Jabri, M., Amar, A., Kali, A., Alrashdi, A., Hadey, C., Boukhlifi, F., 2023. Comparative study on adsorption of crystal violet and chromium (VI) by activated carbon derived from spent coffee grounds. Appl. Sci. 13 (2), 985.
Mahesh, V., 2023. ANN based prediction of the absorption characteristics of additive manufactured glycol-modified polyethylene terephthalate nanocomposites reinforced with short-carbon fibers and nanoclay fillers. Polym. Compos. 44 (12), 8223–8239.
Mahmoud, A.S., Mohamed, N.Y., Mostafa, M.K., Mahmoud, M.S., 2021. Effective chromium adsorption from aqueous solutions and tannery wastewater using bimetallic Fe/Cu nanoparticles: response surface methodology and artificial neural network air. Soil and Water Res. 14, 11786221211028162.
Naseem, T., Bibi, F., Arif, S., Waseem, M., Haq, S., Azra, M.N., Zekker, I., 2022. Adsorption and kinetics studies of Cr(VI) by graphene oxide and reduced graphene oxide-zinc oxide nanocomposite. Molecules 27 (21), 7152.
Nouh, E.S.A., Lasheen, T.A., El-sherif, R.M., Abdel Ghany, N.A., Jebril, E.A., 2019. CeO 2–TiFe 2 O 4 nanocomposite for effective removal of uranium ions from aqueous waste solutions. SN Appl. Sci. 1, 1–13.
Pierotti, R.A., Thomas, H.E., 1974. Virial analysis of low-coverage physical adsorption data on heterogeneous surfaces. J. Chem. Soc., Faraday Trans. 1 70, 1725–1742.
Qi, Y., Wu, W., Han, L., Qu, H., Han, X., Wang, A., Xu, J., 2016. Using TG-FTIR and XPS to understand thermal degradation and flame-retardant mechanism of flexible poly (vinyl chloride) filled with metallic ferrites. J. Therm. Anal. Calorim. 123, 1263–1271.
Rathour, R.K.S., Bhattacharya, J., Mukherjee, A., 2020. Selective and multicycle removal of Cr(VI) by graphene oxide–EDTA composite: insight into the removal mechanism and ionic interference in binary and ternary associations. Environ. Technol. Innov. 19, 100851.
Ren, Y., Han, Y., Lei, X., Lu, C., Liu, J., Zhang, G., Zhang, B., Zhang, Q., 2020. A magnetic ion exchange resin with high efficiency of removing Cr(VI). Colloids Surf. A Physicochem. Eng. Asp. 604, 125279.
Seid, S.M., Gonfa, G., 2022. Adsorption of Cr (V) from aqueous solution using eggshell-based cobalt oxide-zinc oxide nano-composite. Environmental Challenges 8, 100574.
Tadjenant, Y., Dokhan, N., Barras, A., Addad, A., Jijie, R., Szunerits, S., Boukherroub, R., 2020. Graphene oxide chemically reduced and functionalized with KOH-PEI for efficient Cr(VI) adsorption and reduction in acidic medium. Chemosphere 258, 127316.
Tariq, S., Saeed, M., Zahid, U., Munir, M., Intisar, A., Asad Riaz, M., Riaz, A., Waqas, M., Abid, H.M.W., 2022. Green and eco-friendly adsorption of dyes with organoclay: isothermal, kinetic and thermodynamic studies. Toxin Rev. 41 (4), 1105–1114.
Venkatrajan Gopalakannan, V. G., Soodamani Periyasamy, S. P., Natrayasamy Viswanathan, N. V. (2018). Fabrication of magnetic particles reinforced nano-hydroxyapatite/gelatin composite for selective Cr (VI) removal from water.
Weber, T.W., Chakravorti, R.K., 1974. Pore and solid diffusion models for fixed-bed adsorbers. AIChE J 20 (2), 228–238.